PROCEEDINGS, 43rd Workshop on Geothermal Reservoir Engineering
Stanford University, Stanford, California, February 12-14, 2018
SGP-TR-213

Connecting Wellbore and Reservoir Simulation Models Seamlessly Using a Highly Refined Grid

Mitsuo Matsumoto

Exploration & Production Department, Idemitsu Kosan Co., Ltd., 3-1-1 Marunouchi, Chiyoda-ku, Tokyo 100-8321, Japan

mitsuo.matsumoto@idemitsu.com

Keywords: reservoir simulation, wellbore flow

ABSTRACT

The author demonstrates an approach for connecting wellbore and reservoir simulation models. This approach connects these models seamlessly using a highly refined local grid around the wellbore. Applying this approach, we can directly compare observed and simulated bottomhole pressure values at a flowing well without assuming a steady-state flow in the vicinity of the wellbore. This advantage is useful in specifically studying and modeling changes in bottomhole pressure affected by the local distribution of transmissivity near the wellbore.

We consider the transient drop of reservoir pressure caused by a producing wellbore intercepting a fractured zone forming a planar reservoir. The inner boundary of the ring-shaped local grid is along the wellbore surface. The condition of this boundary describes the mass balance at the wellbore surface. The outer boundary refers to the pressure distribution of the global grid dynamically, and the global grid refers to the production rate determined by solving the coupled problem of mass flows in the wellbore and local grid. Using this approach, we successfully simulate an analytic solution that assumes a constant production rate. Finally, an application to a coupled problem of wellbore and reservoir simulation models is demonstrated.

1. INTRODUCTION

Coupled models of mass flows in a wellbore and reservoir are necessary to simulate the production of geothermal fluids through wells under an appropriate condition such as constant wellhead pressure. The key point of these coupled problems is to determine bottomhole pressure accurately. Because numerical grids generally applied to reservoir simulations are too rough to simulate a drop in reservoir pressure in the vicinity of the wellbore, some techniques are required for determining bottomhole pressure. One practical and successful approach is to assume a steady-state mass flow near the wellbore as adopted in the reservoir simulator TOUGH2 (Pruess et al., 1999). In this approach, the productivity index relates the mass flow rate to pressure difference between the bottomhole and reservoir proportionally.

The author has developed another approach that simulates temporal and spatial changes in pressure in the vicinity of the wellbore strictly. For this simulation, we consider a highly refined local grid defined in the vicinity of the wellbore. The changes in pressure on this local grid are simulated efficiently by extending the numerical techniques proposed by Matsumoto (2015). Because flow velocity in the vicinity of the wellbore is high, the quasi-uniform distribution of specific enthalpy on the local grid could be determined by interpolating the values at grid points of the global grid. Therefore, we must solve only the diffusion equation in terms of pressure derived from the conservation equations of mass and enthalpy.

This study describes the mathematical model and numerical techniques used in this approach after a brief review of Matsumoto (2015). A comparison between numerical and analytic solutions at a constant production rate is also provided for validation purposes. Finally, an extension to a coupled problem of wellbore and reservoir simulation models is described.

2. BRIEF REVIEW OF THE FUNDAMENTAL MODEL AND TECHNIQUES

The mathematical model and numerical techniques described in this study are extensions of those proposed by Matsumoto (2015). Through these extensions, we can avoid numerical difficulties in simulating pressure changes on the highly refined local grid such as very large Courant numbers and any explosive increase in computational load.

2.1 Mathematical model

Adopting a Cartesian coordinate system, we describe mass and enthalpy conservation in a single-phase planar (two-dimensional) reservoir model as follows:

$$\partial_t M + U\partial_x M + V\partial_y M = -M\left(\partial_x U + \partial_y V\right) + Q_M \,, \tag{1}$$

$$\partial_t H + U\partial_x H_f + V\partial_y H_f = -H_f\left(\partial_x U + \partial_y V\right) + \lambda\left(\partial_{xx} T + \partial_{yy} T\right) + Q_H \,. \tag{2}$$

The symbols appearing in all equations are defined in the nomenclature at the end of this paper. This nomenclature also gives the mathematical definitions of some symbols. For simplicity, the second term shown in the right-hand side of (2) neglects spatial changes in thermal conductivity. The components of flow velocity U and V obeying Darcy's law are defined as follows:

$$U = k/\phi\mu \cdot \left(-\partial_x P + \rho_f g_x\right), \tag{3}$$

$$V = k/\phi\mu \cdot \left(-\partial_y P + \rho_f g_y\right). \tag{4}$$

Equations (1)–(4) are mathematically identical with the model adopted in the reservoir simulator HYDROTHERM (Kipp et al., 2008) but have different forms for applying general numerical schemes in solving advection problems (e.g., upstream difference, total variation diminishing, and constrained interpolation profile (CIP) schemes). The thermodynamic functions and viscosity of fluid are computed using the equations of state and empirical equation developed by the International Association for the Properties of Water and Steam.

2.2 Numerical techniques

Using the time-splitting method, we advance the advection and non-advection terms of (1) and (2) separately. If the CIP scheme is adopted, we also solve the equations derived when differentiating (1) and (2) regarding x and y as described by Matsumoto (2015). The advection terms are first advanced, followed by the non-advection terms. We then consider the following expressions derived from removing the advection terms from (1) and (2):

$$\partial_t M = -M\left(\partial_x U + \partial_y V\right) + Q_M\,, \tag{5}$$

$$\partial_t H = -H_f\left(\partial_x U + \partial_y V\right) + \lambda\left(\partial_{xx} T + \partial_{yy} T\right) + Q_H\,. \tag{6}$$

The discretized forms of these equations using the finite difference method are advanced semi-implicitly to improve numerical stability. Applying the chain rule, we derive the diffusion equation regarding pressure from (5) and (6) as follows:

$$K_1\partial_t P = K_2\partial_x\left\{k/\phi\mu \cdot \left(\partial_x P - \rho_f g_x\right)\right\} + K_2\partial_y\left\{k/\phi\mu \cdot \left(\partial_y P - \rho_f g_y\right)\right\} + K_3\,, \tag{7}$$

where

$$K_1 = \left(\partial_P M\right)_h\left(\partial_h H\right)_P - \left(\partial_P H\right)_h\left(\partial_h M\right)_P\,, \tag{8}$$

$$K_2 = M\left(\partial_h H\right)_P - H_f\left(\partial_h M\right)_P\,, \tag{9}$$

$$K_3 = -\lambda\left(\partial_h M\right)_P\left(\partial_{xx} T + \partial_{yy} T\right) + Q_M\left(\partial_h H\right)_P - Q_H\left(\partial_h M\right)_P\,. \tag{10}$$

The pressure value at each grid point is determined by advancing (7) implicitly. Referring to these advanced pressure values, (5) and (6) are advanced. Finally, we determine the remaining unknown variables such as specific enthalpy h, temperature T, fluid density ρ_f, and viscosity μ at each grid point. For simplicity, we assume that the properties of rock matrices included in the definitions of M and H (porosity ϕ, density ρ_m, and specific enthalpy c_m) are constant.

3. EXTENSIONS

The aforementioned numerical techniques are extended to simulate temporal and spatial changes in pressure effectively in the vicinity of a producing wellbore. High flow velocity in the vicinity of the wellbore should result in a quasi-uniform distribution of specific enthalpy unless a two-phase region appears and generates the mass fluxes of water and steam that change independently as a result of relative permeability. Therefore, focusing on simulating pressure strictly and estimating specific enthalpy roughly using interpolation is reasonable. In this extension, we adopt a highly refined local grid that expands exponentially as the distance from the well axis increases.

3.1 Pressure change in the vicinity of a wellbore

We apply (7)–(10) to temporal and spatial changes in pressure in the vicinity of a wellbore using a polar coordinate system as follows:

$$K_1\partial_t P = K_2/r \cdot \partial_r\left\{rk/\phi\mu \cdot \left(\partial_r P - \rho_f g_r\right)\right\} + K_2/r^2 \cdot \partial_\theta\left\{k/\phi\mu \cdot \left(\partial_\theta P - r\rho_f g_\theta\right)\right\}. \tag{11}$$

Equation (11) assumes that heat flow resulting from thermal conduction is negligible because that due to advection is high. We also assume that no sources exist that generate in- or outflow in the vicinity of the wellbore. These assumptions result in $K_3 = 0$.

The pressure changes in this polar coordinate system are simulated on the highly refined local grid. To generate this grid, we define physical and computational spaces and adopt coordinate conversion between them. The distance from the well axis r in the physical space is converted to a coordinate ξ in the computational space. The angle θ is defined commonly in both spaces. The relationship between r and ξ is defined as follows:

$$r = \alpha_r \sinh\left(\beta_r \xi\right) + r_w . \tag{12}$$

Using this relationship, a uniform grid defined in the computational space is equivalent to a non-uniform grid that expands exponentially as r increases in the physical space. The same approach is adopted for temporal discretization. The relationship between the physical time t and computational time τ is defined as follows:

$$t = \alpha_t \sinh\left(\beta_t \tau\right). \tag{13}$$

Substituting $\xi_r \partial_\xi$ and $\tau_t \partial_\tau$ for ∂_r and ∂_t, respectively, (11) is redefined in the computational space and time as follows:

$$\tau_t K_1 \partial_\tau P = K_2 / r \cdot \xi_r \partial_\xi \left\{ rk/\phi\mu \cdot \left(\xi_r \partial_\xi P - \rho_f g_r \right) \right\} + K_2 / r^2 \cdot \partial_\theta \left\{ k/\phi\mu \cdot \left(\partial_\theta P - r\rho_f g_\theta \right) \right\}. \tag{14}$$

Equation (14) is advanced using the finite difference method. The grid sizes are uniform in both the ξ and θ directions. The grid size in the ξ direction is unity and that in the θ direction is $\pi/4$. The constants α_r and β_r in (12) are derived from the grid size r_ξ at the wellbore surface ($\xi = 0$) and the pair of reference values, r and ξ. These two relationships yield two non-linear equations with respect to α_r and β_r from (12). We can solve them using the Newton-Raphson method. The computational time-step length is also uniform at unity. The constants α_t and β_t in (13) are determined using the same procedures as those to determine α_r and β_r. Note that the temporal discretization using this approach is also applied to (7) that is defined in the global grid. Thus, the simulated changes in pressure in both the local and global grids are synchronized.

3.2 Connecting the local grid to the wellbore and global grid

The ring-shaped local grid is outlined by inner and outer boundaries, along which r are constant. The inner boundary corresponds to the wellbore surface. In terms of the mass balance at this surface, we obtain the inner boundary condition by the following:

$$q_M = -2\pi\rho_f kwr_w / \mu \cdot \partial_r P \big|_{r=r_w} \tag{15}$$

or

$$q_M = -2\pi\rho_f kwr_w / \mu \cdot \xi_r \partial_\xi P \big|_{\xi=0} . \tag{16}$$

The pressure distribution along the outer boundary is determined by referring to the pressure distribution on the global grid dynamically. Figure 1 illustrates the outer boundary of the local grid superimposed on the global grid. The size of the global grid is partially uniform at Δ in both the x and y directions in the superimposed region. The wellbore in the global grid is represented by a point source corresponding to a single grid point. The outer boundary of the local grid forms a circle whose radius is 2Δ. After the center of this circle at the grid point (i, j) corresponding to the point source in the global grid is located, the pressure value at each grid point along the outer boundary of the local grid is determined based on the values at the grid points in the global grid as follows:

$$P_0 = P_{i+2,j} , \tag{17}$$

$$P_1 = \left(6 - 4\sqrt{2}\right) P_{i+1,j+1} + \left(3\sqrt{2} - 4\right)\left(P_{i+2,j+1} + P_{i+1,j+2}\right) + \left(3 - 2\sqrt{2}\right) P_{i+2,j+2} , \tag{18}$$

$$P_2 = P_{i,j+2} , \tag{19}$$

$$P_3 = \left(6 - 4\sqrt{2}\right) P_{i-1,j+1} + \left(3\sqrt{2} - 4\right)\left(P_{i-2,j+1} + P_{i-1,j+2}\right) + \left(3 - 2\sqrt{2}\right) P_{i-2,j+2} , \tag{20}$$

$$P_4 = P_{i-2,j} , \tag{21}$$

$$P_5 = \left(6-4\sqrt{2}\right)P_{i-1,j-1} + \left(3\sqrt{2}-4\right)\left(P_{i-2,j-1} + P_{i-1,j-2}\right) + \left(3-2\sqrt{2}\right)P_{i-2,j-2}, \tag{22}$$

$$P_6 = P_{i,j-2}, \tag{23}$$

$$P_7 = \left(6-4\sqrt{2}\right)P_{i+1,j-1} + \left(3\sqrt{2}-4\right)\left(P_{i+2,j-1} + P_{i+1,j-2}\right) + \left(3-2\sqrt{2}\right)P_{i+2,j-2}, \tag{24}$$

where bilinear interpolation is adopted to calculate P_1, P_3, P_5, and P_7. The values of specific enthalpy at all grid points in the local grid are determined based on those at the grid points in the global grid and by adopting bilinear interpolation. If the temporal change in the mass flow rate q_M is already known before beginning a run, the global grid refers to nothing in the local grid. In other words, simulations on the global grid can be performed independently. However, if the mass flow rate is determined dynamically based on the bottomhole pressure and specific enthalpy using a wellbore simulation model, the global grid refers to the mass flow rate at each time step. The bottomhole values of the pressure and specific enthalpy are equal to the means of the values at the grid points along the inner boundary of the local grid.

For simplicity in this study, we do not consider skin effects. If we were to consider these effects, we could choose one of two approaches: add the pressure shift based on the skin factor to the aforementioned bottomhole pressure, or define the local distribution of permeability explicitly in the vicinity of the wellbore.

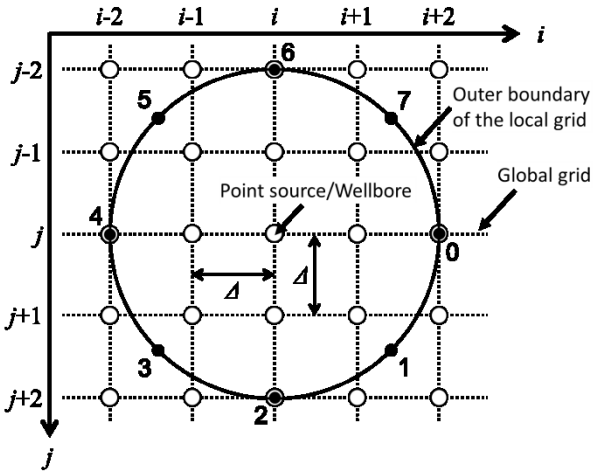

Figure 1: Outer boundary of the local grid superimposed on the global grid. The solid and open points denote grid points in the local and global grid, respectively. The pressure values corresponding to the numbered grid points in the local grid are computed using (17)–(24).

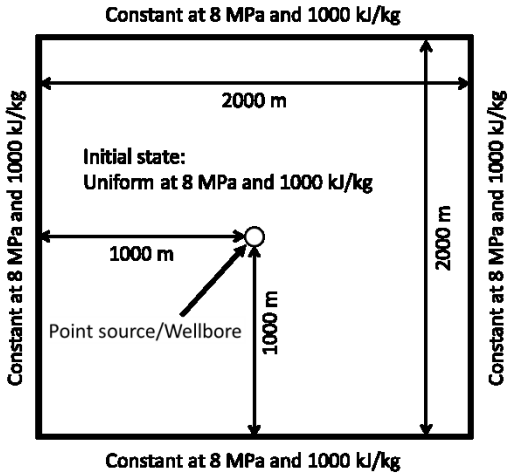

Figure 2: Reservoir model of the numerical solutions.

4. NUMERICAL SOLUTIONS

4.1 Comparison with an analytic solution

Let us consider producing at a constant rate from a square and horizontal reservoir having a side of 2000 m as shown in Figure 2. The reservoir thickness is 100 m. A point source representing a wellbore is located 1000 m from each side. The initial values of pressure and specific enthalpy in the reservoir are uniform at 8 MPa and 1000 kJ/kg, respectively. The pressure and specific enthalpy at each side defining the outer boundary of the reservoir are maintained at these initial values. The production rate is constant at 300 t/h. The physical properties of the rock are uniform as summarized in Table 1. Because of these rock properties and the thermodynamic condition of the reservoir, the transmissivity and storativity are 8.60×10^{-8} m^3/Pa/s and 1.13×10^{-8} m/Pa, respectively. To validate the numerical technique, we refer to the analytic linear solution of the diffusion equation with respect to the pressure derived using these two parameters while assuming that the reservoir expands infinitely (e.g., Dake, 1978).

The size of the global grid covering the entire reservoir is 100 m uniformly. The total number of grid points along each side is 21, including those located at the boundaries. The local grid is defined for simulating temporal and spatial changes in pressure in the vicinity of the wellbore represented by the point source in the global grid. The inner boundary of the local grid is 1.08×10^{-1} m from the point source ($r_w = 1.08 \times 10^{-1}$ [m]). This distance represents a wellbore diameter of 8.5 inches. The outer boundary is two grids (200 m) from the point source as illustrated in Figure 1. The grid size in the r direction at the wellbore surface is 1×10^{-4} m ($r_\xi = 1 \times 10^{-4}$ [m] at $\xi = 0$). The total number of grid points in the r direction is 60 ($r = 200$ [m] at $\xi = 60$). From these two conditions and (12), the non-uniform grid in the r direction is generated as shown in Figure 3. The initial value of the time-step length is 1.37×10^{-13} s ($t_\tau = 1.37 \times 10^{-13}$ [s] at $\tau = 0$). The physical time t reaches 1 d after 4000 steps of time integration ($t = 1$ [d] at $\tau = 4000$). From these two conditions and (13), the time and time-step length at each step are determined. As a result, the time-step length expands to 5.0×10^{-3} d during the first day of the production. The constant time-step length at this value is adopted during the second and later days. The production is terminated at the end of the tenth day. The total number of time steps for 10 days of the production is 5800.

Table 1: Physical properties of the rock.

Permeability	Porosity	Thermal conductivity	Heat capacity of the rock matrix
1×10^{-13} m^2	1×10^{-1}	2.5 W/m/K	2×10^6 J/m^3/K

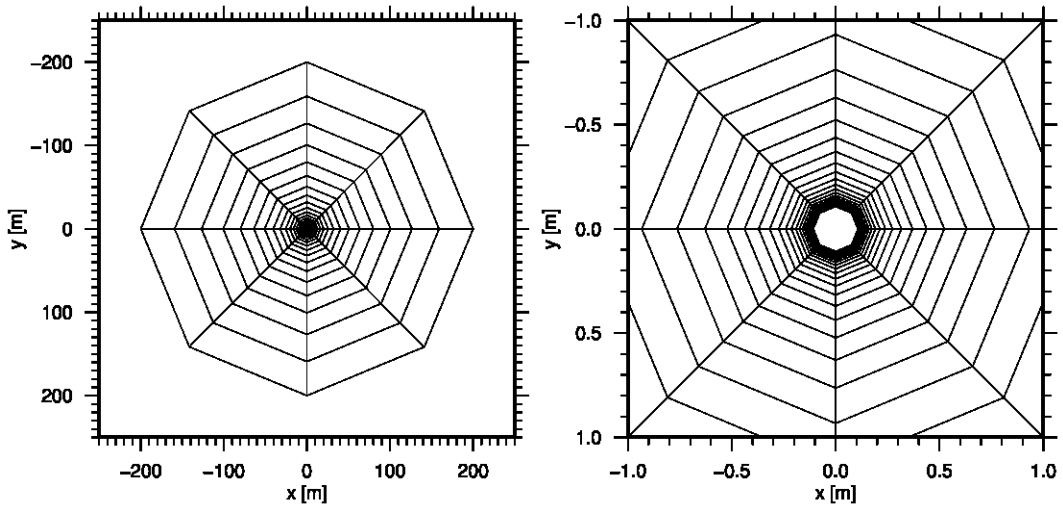

Figure 3: Local grid in the Cartesian coordinate system drawn on different scales. The 8.5-inches wellbore is located at $x = 0$ [m] and $y = 0$ [m].

The numerical and analytic linear solutions of the bottomhole pressure are shown in Figure 4. After an interval of non-linear change, the numerical solution decreases proportionally to logarithmic time. The superimposed analytic linear solution is consistent with the numerical solution. At a time corresponding to the radius of investigation of 1000 m, the numerical solution begins to diverge from the analytic linear solution and converges at a constant value. This change is caused by the boundary condition in which the pressure at the initial value is maintained. From this result, we can prove the validity of not only the temporal and spatial changes in pressure simulated in both the local and global grids but also the connection between these grids.

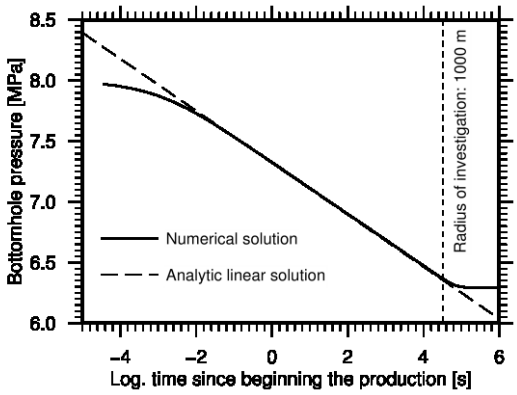

Figure 4: Numerical and analytic linear solutions of the bottomhole pressure for the problem of a constant production rate.

4.2 Extension to a coupled problem of a wellbore and reservoir

We next consider a variable production rate based on the bottomhole pressure as shown in Figure 5a. We assume that this discretized relationship is derived from several observed and/or simulated flows in a production well at a constant wellhead pressure. The aforementioned problem is extended to take into account this variable production rate. In this study, the dependency of the production rate on pressure is considered only for simplicity. That on specific enthalpy can be immediately considered by defining the dependency on both pressure and specific enthalpy.

Currently, the numerical technique of this study determines the production rate explicitly, whereas the pressure value at each grid point is advanced implicitly. Further sophisticated approaches could determine both the production rate and pressure values implicitly. However, explicit determination of the production rate is adoptable for the wide range of practical problems unless very rough time-step lengths are used. The computational load per time step of the semi-implicit scheme adopted in this study is much lower than that of fully implicit schemes widely adopted in multi-purpose reservoir simulators that include solving a large system of non-linear equations.

The simulated changes in the bottomhole pressure and production rate are shown in Figure 5b. The continuous change in the production rate based on the bottomhole pressure is determined using cubic interpolation that refers to four pairs of values of the production rate and bottomhole pressure shown in Figure 5a. Within 1 s from the beginning of the production, the production rate drops from 373 t/h corresponding to the initial bottomhole pressure (8 MPa) to 250 t/h. After this drop in the early time, the production rate gradually becomes stable. The bottomhole pressure becomes approximately proportional to logarithmic time because of this stable production rate. Finally, both the production rate and bottomhole pressure become constant as a result of the boundary condition that maintains the pressure at the initial value.

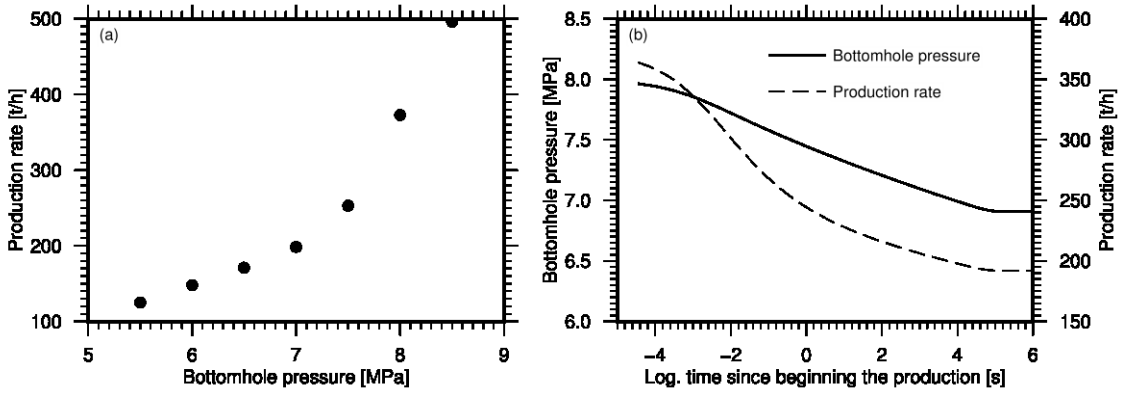

Figure 5: Numerical solution of the coupled problem of a wellbore and reservoir: (a) Relationship between the production rate and bottomhole pressure assumed in the numerical solution. (b) Changes in the bottomhole pressure and production rate.

5. CONCLUSION

In this study, an approach for connecting wellbore and reservoir simulation models using a highly refined local grid was demonstrated. Comparing the numerical solution of this approach with the analytic solution at a constant production rate, we successfully validated the temporal and spatial changes in pressure simulated on the local and global grids as well as the connection between these grids. The variable production rate based on the bottomhole pressure was successfully applied to this approach. By determining the relationship

between the production rate and bottomhole pressure based on observed and/or simulated flows in a production well, we can connect the wellbore and reservoir simulation models successfully.

NOMENCLATURE

Latin symbols

c_m	Specific heat capacity of rock matrices, J/kg/K.
g_x , g_y	x and y component of gravity acceleration in m/s^2.
g_r , g_θ	r and θ component of gravity acceleration in m/s^2.
H	Enthalpy of fluid and rock matrices per unit volume of rocks in J/m^3, $H = \phi\rho_f h + (1-\phi)\rho_m c_m T$.
H_f	Enthalpy of fluid per unit volume of rocks in J/m^3, $H_f = \phi\rho_f h$.
h	Specific enthalpy of fluid, J/kg.
i	Grid index in x direction.
j	Grid index in y direction.
K_1	Refer to (8).
K_2	Refer to (9).
K_3	Refer to (10).
k	Permeability in m^2.
M	Mass of fluid per unit volume of rocks in kg/m^3, $M = \phi\rho_f$.
P	Pressure in Pa.
Q_H	Source flow rate of enthalpy in W/m^3.
Q_M	Source flow rate of mass in kg/s/m^3.
q_M	Mass flow rate of a well in kg/s (negative value for production).
r	Coordinate of the polar coordinate system in m (distance from the well axis).
r_w	Value of r coordinate at the wellbore surface in m.
r_ξ	Grid size in r direction in m, $r_\xi = dr/d\xi$.
T	Temperature in °C.
t	Time in s.
t_τ	Time-step length in s, $t_\tau = dt/d\tau$.
U , V	x and y component of flow velocity in m/s.
w	Thickness of the planar reservoir in m.
x , y	x and y coordinate in m.

Greek symbols

α_r	Constant of coordinate conversion in m.
α_t	Constant of temporal conversion in s.
β_r	Constant of coordinate conversion.
β_t	Constant of temporal conversion.
Δ	Grid size in m.
ϕ	Porosity of rocks.
λ	Thermal conductivity of rocks in W/m/K.
μ	Viscosity of fluid in Pa s.
θ	Coordinate of the polar coordinate system (angle).
ρ_f	Density of fluid in kg/m^3.
ρ_m	Density of rock matrixes in kg/m^3.
τ	Computational time.
τ_t	Derivative of τ regarding t in 1/s, ($\tau_t = d\tau/dt$).
ξ	Coordinate in the computational space.
ξ_r	Derivative of ξ regarding r in 1/m, ($\xi_r = d\xi/dr$).

REFERENCES

Dake, L. P.: Fundamentals of reservoir engineering, Developments in petroleum science, 8, Elsevier, (1978).

Kipp Jr., K.L., Hsieh, P.A., and Charlton, S.R.: Guide to the Revised Ground-Water Flow and Heat Transport Simulator: HYDROTHERM-Version 3, U.S. Geological Survey Techniques and Methods, 6-A25, (2008).

Matsumoto, M.: Application of the Constrained Interpolation Profile (CIP) Scheme to Two-Dimensional Single-Phase Hydrothermal Reservoir Simulations, Geothermics, 54, (2015), 10–22.

Pruess, K., Oldenburg, C. and Moridis, G.: TOUGH2 user's guide, version 2, Lawrence Berkeley National Laboratory Report, LBNL-43134, (1999).